Note: Due to an unfortunate production error, the quantitative estimates (cell sizes, diffusion constants, electrophoretic mobilities) presented in the earlier publication of this manuscript (Stollberg, J., and S. E. Fraser. *J. Cell Biol.* 106:1723–1734) are incorrect. What follows is the correct and intended version. Where applicable please reference this publication, rather than the previous one.

Acetylcholine Receptors and Concanavalin A–Binding Sites on Cultured *Xenopus* Muscle Cells: Electrophoresis, Diffusion, and Aggregation

Jes Stollberg and Scott E. Fraser

Department of Physiology and Biophysics, College of Medicine, University of California, Irvine, Irvine, California 92717

Abstract. Using digitally analyzed fluorescence videomicroscopy, we have examined the behavior of acetylcholine receptors and concanavalin A binding sites in response to externally applied electric fields. The distributions of these molecules on cultured *Xenopus* myoballs were used to test a simple model which assumes that electrophoresis and diffusion are the only important processes involved. The model describes the distribution of concanavalin A sites quite well over a fourfold range of electric field strengths; the results suggest an average diffusion constant of $\sim 2.3 \times 10^{-9}$ cm^2/s. At higher electric field strengths, the asymmetry seen is substantially less than that predicted by the model.

Acetylcholine receptors subjected to electric fields show distributions substantially different from those predicted on the basis of simple electrophoresis and diffusion, and evidence a marked tendency to aggregate. Our results suggest that this aggregation is due to lateral migration of surface acetylcholine receptors, and is dependent on surface interactions, rather than the rearrangement of microfilaments or microtubules. The data are consistent with a diffusion-trap mechanism of receptor aggregation, and suggest that the event triggering receptor localization is a local increase in the concentration of acetylcholine receptors, or the electrophoretic concentration of some other molecular species. These observations suggest that, whatever mechanism(s) trigger initial clustering events in vivo, the accumulation of acetylcholine receptors can be substantially enhanced by passive, diffusion-mediated aggregation.

THE migration of cell-surface molecules is a problem of general interest in developing biological systems. The cell membrane is a fluid matrix consisting of a heterogeneous lipid bilayer, peripheral and integral membrane proteins, and specialized molecular assemblies linking intracellular and membrane-bound components (Singer and Nicholson, 1972; Marchesi, 1985). Many proteins and lipids diffuse freely in the plane of the membrane, and show a globally uniform distribution early in development (Frye and Edidin, 1970; Poo and Cone, 1974; Edidin, 1975). At later stages some of these molecules are concentrated in local regions of the plasma membrane by mechanisms not fully understood. An important example in neurobiology is the induction of acetylcholine receptor (AChR)[1] clusters at the developing neuromuscular junction (see Schuetze and Role, 1987, for review). In this case it is clear that at least some pre-existing, dispersed AChRs are recruited into the forming aggregate (Anderson et al., 1977; Kuromi and Kidokoro, 1984; Ziskind-Conhaim et al., 1984; Role et al., 1985).

A useful technique for the study of macromolecular migration is the in situ electrophoresis of membrane components in response to externally applied electric fields (Jaffe, 1977; Poo and Robinson, 1977; Poo et al., 1978). This technique perturbs molecular distributions independently of cell contacts, and permits quantitative analyses of important migration parameters. In particular, myoball (spherical muscle cell) cultures have been used to advantage in testing theoretical predictions concerning electrophoretic mobility, diffusion, and aggregate stability of concanavalin A (con A) ligand binding sites and AChRs (Orida and Poo, 1978, 1980, 1981; Poo et al., 1979). Because myoballs are nearly spherical, quantitation of component concentration about a two-dimensional perimeter is sufficient to characterize the distribution of the component in three dimensions. In the above-mentioned experiments, electrophysiological and microfluorimetric techniques were used to analyze the distribution of cell surface components after experimental manipulations.

The increased availability of sophisticated computing and video-acquisition hardware has made possible a more detailed analysis of the distribution of cell surface molecules labeled with fluorescent probes. We report here the use of digitally analyzed videomicroscopy to extend the accuracy and resolution of data describing the distribution of con

1. *Abbreviations used in this paper*: α-Bgt, alpha-Bungarotoxin; AChR, acetylcholine receptor; con A, concanavalin A; FLR-con A, fluorescein labeled concanavalin A; TMR-a-Bgt, tetra-methyl-rhodamine labeled alpha-Bungarotoxin.

A-binding sites and AChRs after exposure to electric fields. The use of these techniques permits rigorous comparison to theoretical predictions based on electrophoresis and diffusion. The approach quantitatively demonstrates significant aggregation of AChRs over and above that caused by electric fields; this phenomenon is of great interest in light of the dramatic accumulation of AChRs at the developing neuromuscular junction. Additional experiments examining the requirements for the aggregation phenomenon are also presented.

Materials and Methods

Reagents

Leibovitz's L-15 medium and fetal bovine serum were obtained from Gibco (Grand Island, NY). Collagenase came from CooperBiomedical (Malvern, PA), and fluorescein-labeled concanavalin A (FLR-con A) from Vector Laboratories (Burlingame, CA). Colchicine and cytochalasin B were purchased from Sigma Chemical Co. (St. Louis, MO).

Purified alpha-Bungarotoxin (α-Bgt) was a gift from Drs. Darwin Berg and Stanley Halvorsen. Tetra-methyl-rhodamine-labeled α-Bgt (TMR-α-Bgt) was prepared by the method of Ravdin and Axelrod (1977). In brief the α-Bgt was incubated with tetra-methyl-rhodamine-5(-6)isothiocyanate (Molecular Probes, Inc., Eugene, OR) in 0.1 M Na HCO_3, pH 9.0. The TMR-α-Bgt conjugate was separated and fractionated using Sephadex G-25 and Sephadex CM C-50 chromatographic resins. Peak IV from this latter column was used for all experiments reported here (see Ravdin and Axelrod, 1977).

Culture System

Xenopus laevis embryos were obtained by in vitro fertilization of eggs from a gravid female (O'Rourke and Fraser, 1986), and staged in accordance with Nieuwkoop and Faber (1962). Stage 17–19 embryos were removed from jelly coats and transferred to sterile Steinberg's solution (58.2 mM NaCl, 0.7 mM KCl, 0.4 mM $Ca(NO_3)_2$, 4.6 mM Tris, 50 μg/ml Gentamycin, pH 7.8) containing 1 mg/ml collagenase. The surrounding ectoderm was removed from the dorsal third of the embryo using a tungsten needle, after which the exposed dorsal portion was excised from the rest of the embryo, and left to incubate in the collagenase-Steinberg's solution for ~5 min. Somites were then dissected free of the dorsal aorta, notochord, and neural tube, and transferred to Ca^{++}/Mg^{++}-free Steinberg's solution (58.2 mM NaCl, 0.7 mM KCl, 4.6 mM Tris, 0.3 mM EDTA, 50 μg/ml Gentamycin, pH 7.8). After ~5 min of incubation the cells were collected in a fire-drawn pipette, and transferred to a small volume (e.g., 0.5 ml) of culture medium (85% Steinberg's solution, 10% Leibovitz's L-15 medium, 5% FCS, 50 μg/ml Gentamycin, pH 7.8). The suspension was mixed gently and placed in 2–3-drop aliquots onto clean 24 × 60-mm glass coverslips (Corning Glassworks, Corning, NY) which had been scrubbed in 95% ethanol and air dried. The cultures were kept in 100 × 15-mm plastic petri dishes at 22–24°C in a humidified, darkened chamber for 1–2 d before the experiments.

Electrophoresis

The electrophoresis chambers were modeled after those described previously (Peng and Jaffe, 1976; Poo et al., 1978; see Fig. 1). Two 7 × 60-mm coverslip runners were cut and cemented along the long edges of 1 × 3-in glass slides (Sargent-Welch, Skokie, IL). Coverslips on which myoballs had been cultured were inverted and affixed to the runners with vacuum grease (Dow Corning, Pasadena, CA) to complete the chambers, with internal dimensions of 60 × 10 × 0.2-mm.

Voltage potentials were regulated with an electrophoresis power supply (Instrumentation Specialties Company; model No. 493). The voltage source was connected through a switching-resistor box and Ag/AgCl wires immersed in 60 × 15-mm petri dishes containing Steinberg's solution (see Fig. 1). The electrical path through the chamber was completed by U-shaped 6-mm (I.D.) glass tubes filled with 2% agar/Steinberg's solution, which contacted the chamber via electrolyte puddles at either end. Except where noted, Steinberg's solution was used for the puddle and chamber electrolyte. Smaller agar bridges were formed with plastic tubing and used with Ag/AgCl inserts to monitor directly the potential drop across the chamber (see Fig. 1). Delivered voltages were measured using a Keithley model 169 multimeter (Cleveland, OH). The chambers were placed on sheet metal heat sinks, and the bridges were stabilized with modified 100 × 15-mm petri dish lids. The apparatus permitted delivery and monitoring of 6 different fields to 6 chambers.

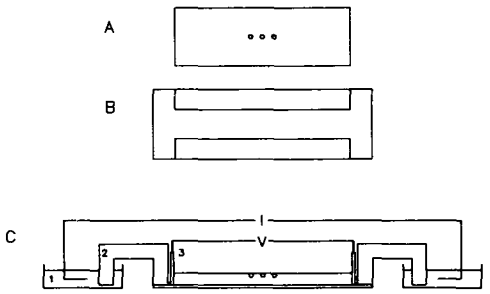

Figure 1. Diagram of the electrophoresis apparatus (*A*) myoball culture on glass coverslip. (*B*) glass slide with coverslip runners. (*C*) side view of assembled chamber and associated apparatus. (*I*) Current source connected through Ag/AgCl wires in Steinberg's solution (*1*) and agar/Steinberg's solution filled glass bridges (*2*). (*V*) voltmeter for monitoring field strength connected via agar/Steinberg's solution Ag/AgCl plastic tubing bridges (*3*). For purposes of clarity the electrolyte puddle at either end of the chamber has been omitted, and chamber depth has been shown magnified.

Fluorescent Labeling

After the electrophoresis (and in some cases a specified post-field period), the chambers were rapidly chilled and maintained on ice. The cells were incubated for 10 min with Steinberg's solution containing (*a*) 25 μg/ml FLR-con A, (*b*) 300 nM TMR-α-Bgt with 25 μg/ml unlabeled con A, or (*c*) 300 nM TMR-α-Bgt with 25 μg/ml FLR-con A (double label experiments). The cultures were then rinsed three times with 300 μl Steinberg's solution, and left on ice until commencement of videomicroscopy. As a control for autofluorescence and non-saturable binding, several cultures were labeled in the presence of excess unlabeled ligand. For both FLR-con A and TMR-α-Bgt, the nonspecific signal obtained was less than 10% of the total signal seen in sister cultures. These estimated nonspecific signals have been subtracted from experimental data.

Videomicroscopy

Cells were imaged through a Zeiss Universal microscope using a Neofluor 40× objective with epi-illumination for fluorescence, and filter sets appropriate to excitation and emission spectra for fluorescein and rhodamine. Occasional cultures in which cells did not appear robust and phase-bright after electrophoresis were not used for quantitative analysis, nor were individual cells deviating substantially from sphericity. Optical images were gathered by a SIT video camera (RCA; Lancaster, PA model No. TC1030) and stored on video cassettes (Sony U-matic video cassette recorder [Tokyo, Japan]; models VO-5600 and VO-5800).

Image Digitization and Acquisition

Analog videotape images were converted to digital images using a Digisector DS-88 board (Microworks, Del Mar, CA) modified by the addition of a 10-turn potentiometer to permit decreased contrast settings. The video image was digitized with a resolution of 256 × 256 pixels per screen, and a grey scale of 0–255. At the magnification used in these experiments, each pixel represented ~1 μm. The DS-88 board was used in conjunction with an American Micro Technology computer (model No. AMT 286; Santa Ana, CA), which performed all image analyses. To minimize deviations in response over the video field (see below), all scans were confined to a 100 × 100 pixel region in the center of the screen. All images were acquired as the average of 10 scans.

Spatial aberrations in illumination and viewing optics, and in camera sensitivity, were corrected by use of three "flatfield" images gathered in the absence of cells. One image was taken with the light path closed (camera noise only), while the other two were views of low and high concentrations (e.g. 5 μg/ml and 25 μg/ml) of FLR-con A in the electrophoresis chambers. The flatfield images were acquired separately for each experiment.

Correction of cell images was made on a pixel-by-pixel basis assuming

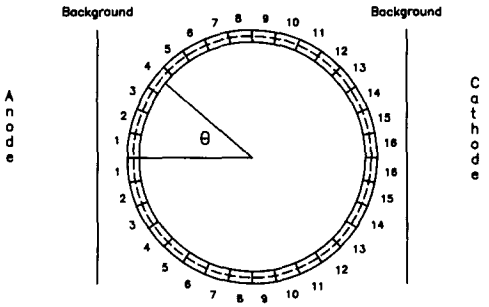

Figure 2. Schematic illustrating the geometrical analysis of a cell image. *Anode* and *cathode* designate the orientation of the cell with respect to the electric field. The dashed-line circle indicates the boundary of the cell image. The solid circles represent the tolerance (±5% of the radius) within which pixels must lie to be accepted. For each pixel within this tolerance, the angle from the anode (θ) is found and the corrected intensity (less background) is sorted into one of 16 sectors representing θ. Note that although the sectors comprise equal angles (11.25°) in two dimensions, the regions on a sphere represented by the sectors vary considerably in area. For simplicity the description and schematic assume the circularity of the image. In fact the software made the more general approximation of an ellipse with axes oriented horizontally and vertically.

a linear input-output relationship defined by the low and high flatfields. Pixels were rejected (not included in the analysis of a given image) if the uncorrected intensities found in these two flatfields were within 10% of each other, or if in either flatfield the 10 scans showed a standard error greater than 15%. The rejection scheme typically discarded 5–25 pixels out of the ~2,500 making up the cell image. The null flatfield, taken with the optical path closed, was used to insure that illumination, brightness, and contrast settings were such that observations were in the linear range of the assay.

Geometrical Analysis of Image

Before digital conversion of an image the left, right, top, and bottom boundaries of the cell were specified via cursor positioning on the video monitor. A rectangular scan was then performed to include the cell image with a 7-pixel margin along each border. Given the boundaries of the cell, the software identified those pixels falling within ±5% of the cell radius, and calculated the angle relative to the applied field subtended by each of them (see Fig. 2). The intensity scored at each pixel was then corrected, and the (corrected) background intensity found along the left and right margins of the image was subtracted. The resulting estimates of light intensity were summed into the appropriate sectors (16 in all) representing different angles (see Fig. 2). When all pixel intensities within the ±5% annulus were summed, the intensity corresponding to each sector was divided by the number of pixels within it to give the average intensity of the sector. This average was used as the estimate of binding site concentration within the region of the sphere's surface sampled by the sector. These regions are bounded by concentric circles (lines of latitude) perpendicular to the electric field, and have areas ranging from ~1% (sectors 1 and 16) to 10% (sectors 8 and 9) of the total surface area of the sphere.

The total fluorescent label on each cell was approximated by the sum of the cell's sector intensities weighted by the cell-surface area represented by each sector. To facilitate comparison of distributions between cells, this total label value was used to normalize each cell's sector intensities such that the normalized total label on each cell was the same. Analysis of the cells on a given slide was completed by finding the average value (over n cells) of the normalized sector intensity for each sector. These means were used as the estimates of ligand site concentration at each sector, and expressed as a percent of the average concentration of sites.

To compare the extent of redistribution under different conditions, a simplifying analytical representation called the Asymmetry index (A) was used (Orida and Poo, 1977; Poo et al., 1979). The Asymmetry index summarizes the relative concentrations at the anode (C_0) and cathode (C_{180}) facing poles of a cell, and is defined as $A = (C_{180} - C_0)/(C_{180} + C_0)$. The index was calculated using intensities at the 1st and 16th sectors as approximations to C_0 and C_{180}, respectively (see Fig. 2).

Statistics and Curve-fitting

In tabulating data for the figures, the means of each data point for each experiment were averaged, and the standard error of each grand average (n = 3–8 experiments) was taken to account for possible increased variability between experiments.

Unless otherwise indicated, curves were fit to data by the Levenberg-Marquardt method; error estimates on fit parameters are not true standard errors, but rather corresponding estimates derived from the fitting procedure (cf. Press et al., 1986). Chi-square values are reported in the format χ^2 (degrees of freedom) = value, as an objective measure of the correspondence between curves and data.

The Model

The basic model under test in these experiments is one put forward by Jaffe (1977) and elaborated on by Poo and collaborators (Poo et al., 1979; McLaughlin and Poo, 1981). The simplifying assumptions are (*a*) that the cell is approximated by a non-conducting sphere, and (*b*) that the two processes dominating the molecular distribution are electrophoresis[2] and diffusion. Given these assumptions, the cell radius (r), the initial molecular concentration (C_i), the field strength (E), the pseudo-electrophoretic mobility constant (m), and the diffusion constant (D), the steady-state concentration as a function of θ (C_θ) is

$$C_\theta = \alpha \cdot \exp(-\beta \cdot \cos\theta),$$

where

$$\alpha = \beta \cdot C_i/\sinh(\beta),$$

and

$$\beta = 1.5 \cdot E \cdot r \cdot \frac{m}{D}.$$

An additional term (f_m) is introduced to represent the fraction of sites which are mobile in the plane of the membrane. The equation describing steady-state distributions is therefore

$$C_\theta = f_m \cdot \alpha \cdot \exp(-\beta \cdot \cos\theta) + (1\text{-}f_m) \cdot C_i,$$

where (m/D) and f_m can be allowed to vary in fitting the data (all other parameters being measured quantities).

Results

Verification of Techniques

The data presented below depend on the validity of using intensity estimates from video images as a measure of relative ligand binding site concentrations. To test the estimation procedure, a range of FLR-con A concentrations were prepared, placed in electrophoresis chambers, and videotaped under the same conditions used in actual data collection. These records were analyzed with the described software as if an average-size (20 μm radius) cell image was present.[3] Fig. 3 *a* shows the average corrected intensity found along the "cell perimeter" as a function of the concentration of dye used. The corrected value is seen to be proportional to the FLR-con A concentration up to ~60 μg/ml, after which it begins to plateau.

The proportional relationship between average corrected intensity and dye concentration does not rule out systematic deviations in sensitivity over the spatial field. Such variation, masked in the averages, would hamper interpretation of data

2. McLaughlin and Poo (1981) have suggested that the driving force is electro-osmotic, rather than purely electrophoretic. This does not change the form of the model.

3. The background subtraction was suppressed, as there is no distinction between image and background in this case.

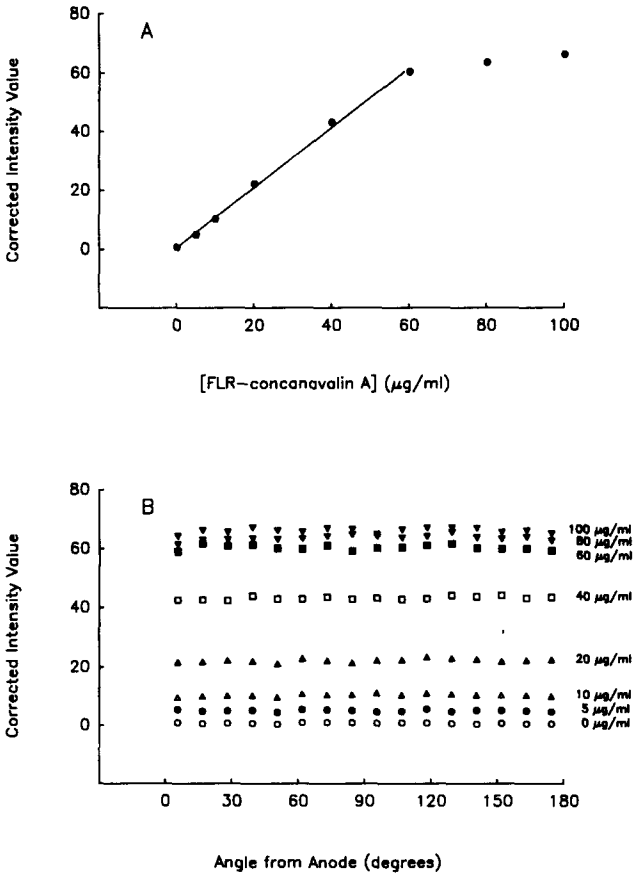

Figure 3. Results from digital analysis of flatfields. Electrophoresis chambers were filled with the indicated concentrations of FLR-con A and scanned as if they contained an average-size cell near the center of the screen. Intensity data were corrected using separate scans of 5 and 60 μg/ml FLR-con A for the low and high flatfields, respectively. (*A*) Average corrected intensity over the entire annulus vs. FLR-con A concentration. The curve is a linear regression fit to the first six data points. (*B*) Re-plotting of the data showing corrected intensity as a function of θ for the eight concentrations examined.

with respect to the relative distribution of sites around a cell perimeter. Fig. 3 *b* shows the corrected intensity as a function of perimeter position for the uniform dye concentrations described above. It is seen that there is little variation over the spatial field in the linear range of the assay. All experiments with fluorescently labeled cells were conducted within this linear range, as determined by uncorrected pixel intensities.

Another consideration is the choice of the "tolerance" or width of the annulus used in image analysis (expressed here as a percentage of the radius; see Fig. 2). Several sets of records were analyzed with tolerances ranging from 1.5–20%. A comparison of the resulting asymmetry indices showed a tendency for the index to increase as the tolerance was decreased; the index changed ~10% over the full range evaluated (data not shown). A tolerance of 5% was chosen as a compromise permitting close perimeter following, and stability of results with respect to slight mis-positioning of the annulus.

Correct interpretation of the data also depends on approximate sphericity of the cells. Accordingly, only cells nearly circular in cross-section were selected for analysis. Use of a calibrated fine focus to measure the distance between the adhesion surface and free surface of cultured cells indicated that the diameters parallel and orthogonal to the plane of focus were approximately the same (data not shown). There was no evidence of any shape changes in the plane of focus induced by the exposure to electric fields, which would skew interpretations predicated on sphericity. In a sample comparing cells exposed to no field vs. cells exposed to 8 V/cm for 40 min, we found horizontal radius = 20.4 ± .8 μm, vertical radius = 20.2 ± .6 μm, vs. 19.8 ± .8 μm and 19.8 ± .6 μm, respectively (4 experiments in each condition, 8–12 cells per experiment).

A final methodological concern is the use of con A or FLR-con A in conjunction with cold to stabilize molecular distributions. Although con A can partially block α-Bgt binding (Boulter and Patrick, 1979), the expected effect is less than 10% under the conditions used, and does not affect the assessment of *relative* AChR concentrations. Pretreatment of cultures with con A eliminated field-induced accumulation of AChRs (Fig. 11), and pre-labeling with FLR-con A greatly diminished the field-induced accumulation of con A sites (Fig. 12). Additionally, control experiments demonstrated the stability of asymmetries in FLR-con A and TMR-α-Bgt binding after treatment with con A (data not shown). The ability of con A to stabilize the measured site distributions rules out the possibility that autofluorescent elements (e.g., yolk granules) contribute significantly to the measurement.

FLR-Con A–labeling Studies

The development of con A–binding site asymmetry, expressed as Asymmetry index vs. time in the electric field, is shown in Fig. 4. The approach to steady-state is well fit by an exponential with $\tau \approx 12$ min. On the basis of these data, 40 minutes was selected as the standard field duration for steady-state experiments (see below). Assuming the general model under consideration (see Materials and Methods), Poo (1981) has shown that the approach to steady-state is approximated by an exponential with time constant $\tau = r^2 (1 - 0.1 \cdot \beta^2)/(2) \cdot D$. Given $m/D = 128\ V^{-1}$ (see below), $r =$

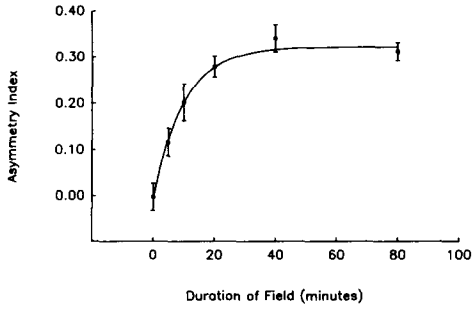

Figure 4. Development of concanavalin A–binding site asymmetry. Cells were subjected to an electric field of 8 V/cm for varying amounts of time, and analyzed for asymmetry as described. Data represent means ± standard errors of three experiments, each consisting of 8–10 scanned cells. The curve is the least-squares fit of an exponential to the data. The time constant is 12 ± 4 min; $\chi^2_{(3)} = 0.7$. A similar time course for development of asymmetry was seen at 4 V/cm.

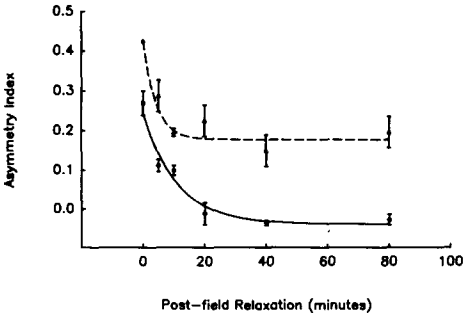

Figure 5. Relaxation of field-induced asymmetry in concanavalin A-binding sites. Cultures were exposed to 4 V/cm (*circles*) or 8 V/cm (*triangles*) for 40 min, and given the indicated amounts of time at room temperature before labeling and analysis. The curves represent least-squares fits of the data to an exponential decay. At 4 V/cm the time constant is 14 ± 4 min with $\chi^2_{(3)} = 8.2$; at 8 V/cm the time constant is 4 ± 1.6 min with $\chi^2_{(3)} = 3.0$.

20 μm, and $E = 8$ (V/cm, β is ~1.5. Together with the observed τ, this corresponds to an estimate of $D \approx 2.2 \times 10^{-9}$ cm²/s.

The relaxation of con A-binding sites after exposure to electric fields is depicted in Fig. 5. Cultured cells were subjected to fields of 4 and 8 V/cm for 40 min, and then given varying amounts of time to relax. Given the assumptions of the model, it can be shown that the decay of asymmetry is approximated by an exponential with $\tau = r^2/2 \cdot D$ (Huang, 1973). The relaxation from 4 V/cm shows $\tau \approx 14$ min, which yields $D \approx 2.4 \times 10^{-9}$ cm²/sec, in good agreement with the estimate of D obtained from the development of asymmetry during exposure to fields. Relaxation from asymmetries induced at 8 V/cm were markedly incomplete.

Representative video images of cells showing steady-state distributions of con A sites are shown in Fig. 6. Con A-binding sites accumulated at the cathode end of cells, and they displayed a continuous gradation in concentration around the cell perimeter. A critical prediction by the model under consideration is that the same values for the parameters m/D and f_m should fit data for the distributions of sites at different voltage gradients. Fig. 7 shows the data and fitted curves for steady-state distributions at field strengths of 0, 1, 2, and 4 V/cm. As the data are fit well with the same parameter values, the results support the theoretical model. The experiments indicate estimated parameter values of $m/D = 64$ V⁻¹, $f_m = 0.48$ (*solid curves*). The dashed curves represent the best fit to m/D assuming all of the binding sites are mobile ($f_m = 1.0$). The similarities between the solid and dashed curves, and the insubstantial change in the corresponding χ^2 values (see legend to Figure 7), suggest that these data cannot be used to estimate f_m with any precision.

Steady-state experiments were also carried out at 8 V/cm (Fig. 8). Under these conditions the discrepancy between the data and the family of curves from Fig. 7 is conspicuous. At this higher field strength the solid and dashed curves, generated from the measurements in Fig. 7, are noticeably different from each other. However, neither curve is an adequate approximation to the data of Fig. 8. The dotted curve in Fig. 8 represents a readjustment of the two parameters to give a maximum likelihood fit to the data. This fit is quite good, underscoring the lack of testability inherent in examination of data from a single field strength.

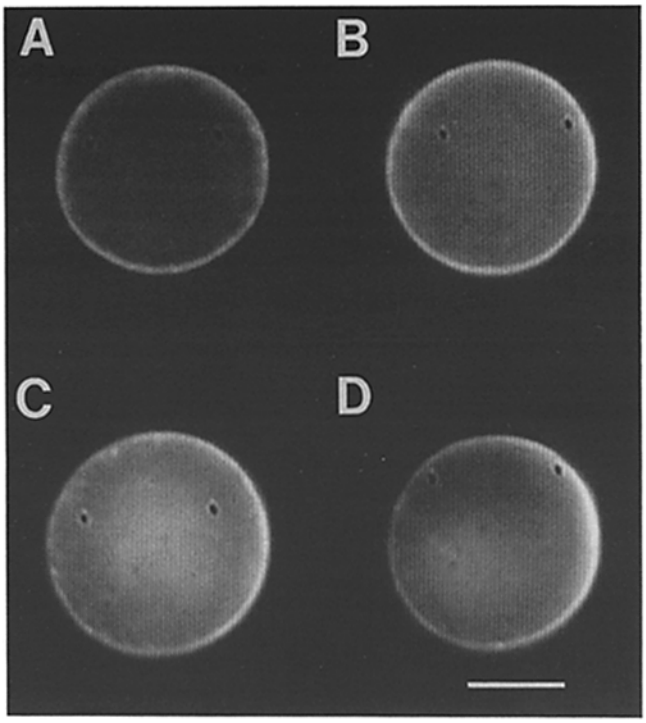

Figure 6. Representative video images of cells exposed to electric fields under steady-state conditions. Cells were exposed to the indicated electric fields for 40 min, and then labeled with FLR-con A. (*A*) 0 V/cm. (*B*) 1 V/cm. (*C*) 2 V/cm. (*D*) 4 V/cm. Individual micrographs reveal cell-to-cell variation in overall brightness, and occasional bright foci unrelated to experimentally induced migration. These effects are minimized by the normalization and averaging procedures in the quantitative analysis of multiple images (see Materials and Methods). The prominent dark spots result from flaws in the camera tube; these along with other faulty pixels were rejected in the analysis (see Material and Methods). In all cases the field cathode is to the right. Bar, 20 μm.

TMR-α-Bungarotoxin-labeling Studies

Analysis of the distribution of AChRs after electric fields demonstrated that the model assumptions (electrophoresis and diffusion as the only important processes) were not met by the experimental system. The development of AChR asymmetry during exposure to fields is not well fit by a single exponential (data not shown). Fig. 9 shows the substantial asymmetry arising from a field of 8 V/cm for 80 min. The best-fit model parameters do not satisfactorily describe this distribution, or the qualitatively similar distributions seen after fields of 4 V/cm. Analysis of the data from Fig. 9 suggests a diffusion-trap mechanism of AChR aggregation (see Discussion), and control experiments indicated that accumulation of the receptor does indeed continue after the electric field is turned off (see below).

Double labeling studies of Postfield AChR Accumulation: Control Experiments

A standard field/postfield protocol was chosen to study the postfield aggregation of AChRs. Under this paradigm comparisons were made between two conditions: (*a*) "field"–cells subjected to a field of 4 V/cm for 20 min, and (*b*) "post-

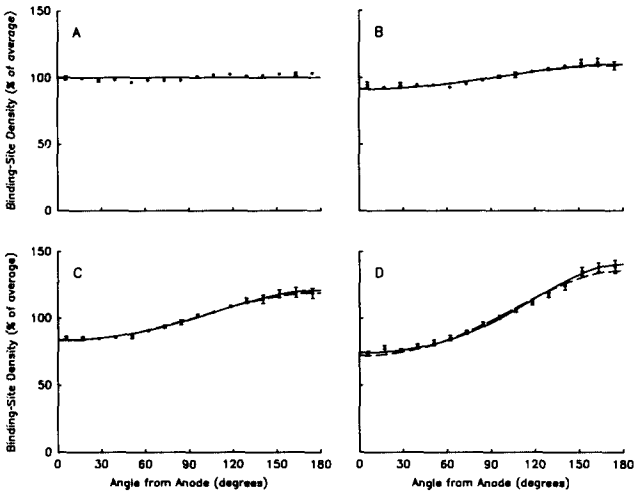

Figure 7. Steady-state distributions of concanavalin A-binding sites after electrophoresis at 0–4 V/cm. Cultures were subjected to the indicated electric fields for 40 min and analyzed for the distribution of con A-binding sites as described. Data represent means ± standard errors for 3–6 experiments, each consisting of 7–14 scanned cells. Solid curves shown are the least-squares fit of the predicted distribution to the combined data from *B*, *C*, and *D* (see Materials and Methods, The Model). The fit parameters are $m/D = 64 \pm 8\ V^{-1}$ and $f_m = 0.48 \pm .05$; $\chi^2_{(45)} = 67$. Dashed curves represent the least-squares fit to the data assuming the mobile fraction $f_m = 1.0$. The fit parameter m/D is then $34 \pm .5\ V^{-1}$; $\chi^2_{(46)} = 81$. (*A*) 0 V/cm. (*B*) 1 V/cm. (*C*) 2 V/cm. (*D*) 4 V/cm.

field"–cells treated as in (*a*) and then given 40 min at room temperature for post-field redistribution. In either case the experiment was terminated by chilling and labeling the cultures with FLR-con A and TMR-α-Bgt, and analyzed using filter sets selective for the respective dyes. Control experiments demonstrated that the signal from either dye was insignificant when using filters appropriate to the other (data not shown).

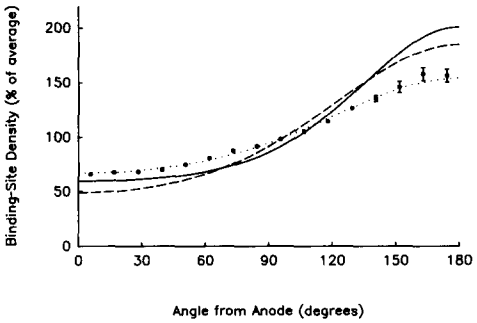

Figure 8. Steady-state distribution of concanavalin A-binding sites after electrophoresis at 8 V/cm. Cultures were exposed to electric fields of 8 V/cm for 40 min and analyzed for the distribution of con A-binding sites as described. Data represent means ± standard errors for eight experiments, each consisting of 7–12 scanned cells. The solid and dashed curves represent the predicted distribution from the model given the measurements from Fig. 7 (*solid*; $m/D = 64\ V^{-1}$, $f_m = 0.48$, $\chi^2_{(15)} = 524$; *dashed*: $m/D = 34\ V^{-1}$, $f_m = 1.0$, $\chi^2_{(15)} = 867$). The dotted curve is the 2-parameter least-squares fit to this data, yielding $m/D = 34 \pm 4\ V^{-1}$ and $f_m = 0.56 \pm .05$; $\chi^2_{(13)} = 14.0$. Note that the scale of this graph is different from those in Fig. 7.

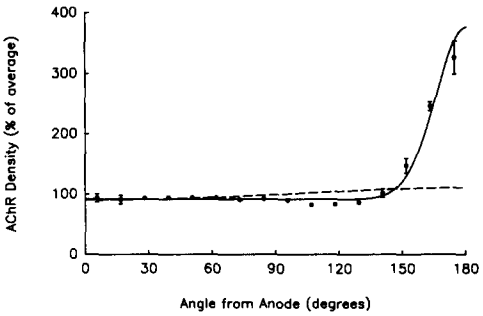

Figure 9. Distribution of acetylcholine receptors after exposure to an electric field. Cultures were exposed to a field strength of 8 V/cm for 80 min, then labeled with TMR-α-Bgt and analyzed as described. The solid curve represents the 2-parameter least-squares fit of the model distribution to this data; $m/D = 831 \pm 83\ V^{-1}$, $f_m = 0.084 \pm .002$, $\chi^2_{(13)} = 170$. The dashed curve was fit by eye to the left-most data points to give a qualitative assessment of the electrophoretic component in this distribution (see Discussion); $m/D = 10\ V^{-1}$, $f_m = 0.5$. Note the markedly different scale from those of Figs. 7 and 8.

Postfield accumulation of AChRs was seen in almost all cells from control experiments. Typical videomicrographs illustrating the phenomenon are shown in Fig. 10 along with views of the same cells depicting con A site distributions. The AChRs continue to aggregate at the cathode-facing pole during the postfield period (cf. Fig. 10 *f* and *e*), while the con A sites relax back towards symmetry over the same interval (cf. Fig. 10 *c* and *b*). Quantitation of the asymmetries in TMR-α-Bgt and con A-binding sites under the field/postfield paradigm are shown in Figs. 11 and 12, respectively.

Pre-labeling and Cross-linking Experiments

Two kinds of experiments were undertaken to establish whether the observed postfield increase in asymmetry was in fact due to aggregation of preexisting AChRs, rather than to preferential expression of new AChRs. In the first set of experiments, cells were labeled with TMR-α-Bgt and then subjected to the standard experimental protocol. As seen in Fig. 11, pre-labeled AChRs show both field and post-field asymmetries indistinguishable from controls. In another set of experiments, cells were incubated with con A to cross-link existing AChRs, after which the cells were subjected to the protocol. Fig. 11 shows negligible electrophoresis or postfield accumulation of AChRs under these conditions, indicating that the accumulation phenomenon depends on the mobility of pre-existing AChRs. Fig. 12 demonstrates a substantial decrease in field-induced asymmetry of con A sites when the cells are labeled before the field.

Trypsin Experiments

Three sets of experiments were undertaken to analyze the effects of trypsin during, before, and after the field/postfield protocol. Cells treated with trypsin for 1 h before, and throughout the experiment, showed drastically reduced AChR asymmetries in both field and postfield conditions (Fig. 11). To ascertain whether this reduction depends on the presence of trypsin during the accumulation of AChRs, cells were incubated with trypsin, rinsed extensively, and then

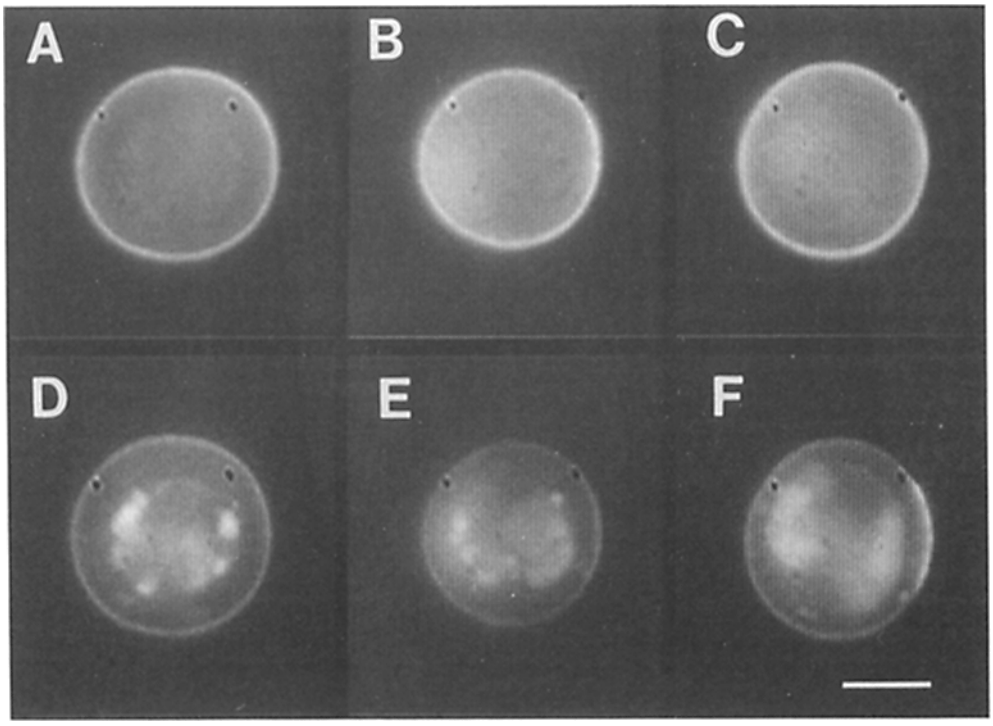

Figure 10. Representative video images of cells subjected to electric fields with and without subsequent relaxation. Cultured cells were subjected to the indicated protocol and labeled with both FLR-con A and TMR-α-Bgt. (*A–C*) cells viewed with fluorescein filters to reveal con A–binding sites. (*D–F*) The same cells as *A–C* viewed with rhodamine filters to reveal TMR-a-Bgt–binding sites. (*A* and *D*) No field. (*B* and *E*) 4 V/cm for 20 min. (*C* and *F*) 4 V/cm for 20 min followed by 40 min postfield relaxation. Individual micrographs reveal cell-to-cell variation in overall brightness, and occasional bright foci unrelated to experimentally induced migration. These effects are minimized by the normalization and averaging procedures in the quantitative analysis of multiple images (see Materials and Methods). The fluorescent areas inside the cell perimeters in *D–F* are due to yolk granules within the cells; these exhibit more autofluorescence under the illumination conditions for rhodamine than under those for fluorescein. The prominent dark spots result from flaws in the camera tube; these along with other faulty pixels were rejected in the analysis (see Material and Methods). In all cases the field cathode is to the right. Bar, 20 μm.

subjected to the field/postfield protocol. Under these conditions the AChR accumulation was similarly reduced (Fig. 11). In the final set of experiments cells were subjected to the field, and then incubated with trypsin during the postfield period. These cultures showed a significant decrease in postfield asymmetry when compared to controls (Fig. 11). The effects of trypsin do not result from a loss of TMR-α-Bgt–binding sites because (*a*) analysis of the total amount of labeling shows no such decrease and (*b*) trypsin-treated cultures displayed a twitch response to acetylcholine, which could be blocked by α-Bgt (data not shown). The various trypsin treatments had no significant effect on con A site distributions under the field/post-field paradigm (Fig. 12).

The Role of Calcium

To investigate the possible role of calcium in the field-induced accumulation of AChRs, cells were incubated for 1 h before experimentation, and maintained throughout the experiment in Ca^{++}-free Steinberg's solution. As seen in Fig. 11, cells treated in this manner showed a small decrease in the field-induced accumulation of AChRs, and a substantial reduction in the postfield accumulation. Ca^{++}-free Steinberg's solution had no effect on the con A sites under these conditions (Fig. 12). To determine whether the effect on AChR accumulation is reversible, cells were incubated for 1 h in Ca^{++}-free Steinberg's solution, rinsed and incubated 1 h in Steinberg's solution, and then subjected to the experimental protocol. Fig. 11 shows a significant increase in the postfield accumulation as compared with cultures in Ca^{++}-free buffer throughout the experiment. Thus the effects of low calcium are substantially reversed within 1–2 h.

The Role of Microtubules and Microfilaments

To determine whether cytoskeletal elements are necessary for the postfield aggregation of AChRs, cells were treated with drugs to disrupt microtubules and microfilaments. Cultures were incubated with 20 μM colchicine or 20 μM cytochalasin B for 2 h before and throughout the course of experiments. Neither drug had significant effects on the redistribution of AChRs (Fig. 11) or con A sites (Fig. 12) in response to the field/postfield protocol.

Discussion

Methodological Considerations

The results presented in this paper rest on the assumption that corrected intensity estimates accurately reflect the redistribution of preexisting ligand binding sites over the cell surface. This in turn is based on linearity of the assay for ligand concentration. As shown in Fig. 3, the assay is quite linear over a substantial range of ligand concentrations. Analysis of experiments was performed only when the data were within that linear range. Under some conditions a multivalent ligand, such as con A, may bind nonlinearly with respect to site density. In this case the total number of sites would appear to change as the distribution of sites increased in asymmetry. As a check on this possibility, total con A binding (the

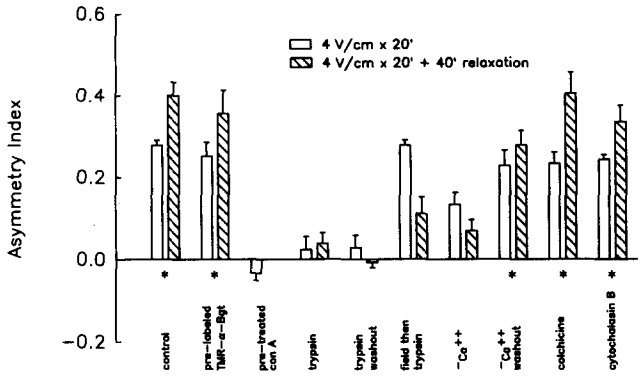

Figure 11. The effects of treatments on the electrophoresis and postfield aggregation of acetylcholine receptors. Cultures were treated as indicated and subjected to a field of 4 V/cm for 20 min with and without an additional 40 min postfield at room temperature. Except where noted, the cells were then double labeled and analyzed as described. Control, no additional treatment. Pre-labeled TMR-a-Bgt, labeled with 300 nM TMR-a-Bgt for 10 min at 22°C before experiments (no further labeling). Pre-treated con A, incubated with 25 μg/ml con A for 10 min at 22°C, then subjected to the field and labeled with TMR-a-Bgt. -Ca^{++}, incubated in Ca^{++}-free Steinberg's solution (58.2 mM NaCl, 0.7 mM KCl, 1.3 mM MgSO4, 0.4 mM EGTA, 4.6 mM Tris, 50 μg/ml Gentamycin) 1 h before and throughout experiment. -Ca^{++} washout, incubated for 1 h in Ca^{++}-free Steinberg's solution, then 1 h in Steinberg's solution before experiment. Trypsin, incubated in 0.1% trypsin/Steinberg's solution 1 h before and throughout experiment. Trypsin washout, incubated in 0.1% trypsin/Steinberg's solution for 1 h, then returned to Steinberg's solution immediately before experiment. Field then trypsin, after electrophoresis placed in 0.1% trypsin/Steinberg's solution for the postfield period (*hatched bar*); the blank bar is a reprinting of the control for this condition. Colchicine, cytochalasin B, incubated 2 h before and throughout experiment in 20 μM of the respective drug. Data represent the means ± standard errors of 3–6 experiments, each consisting of 5–9 cells. (*) Indistinguishable from controls (both field and post-field) on the basis of one-factor ANOVA F tests (field, F[4/13] = 0.61; postfield, F[4/14] = 1.52). Within this "control" group, field vs. postfield asymmetry values are significantly different (0.247 ± .009 vs. 0.355 ± .023; $p < .001$, *T* test). The control group field and postfield values are significantly different from those in the trypsin group ($p < 0.005$) and the -Ca condition ($p < .025$, *T* tests).

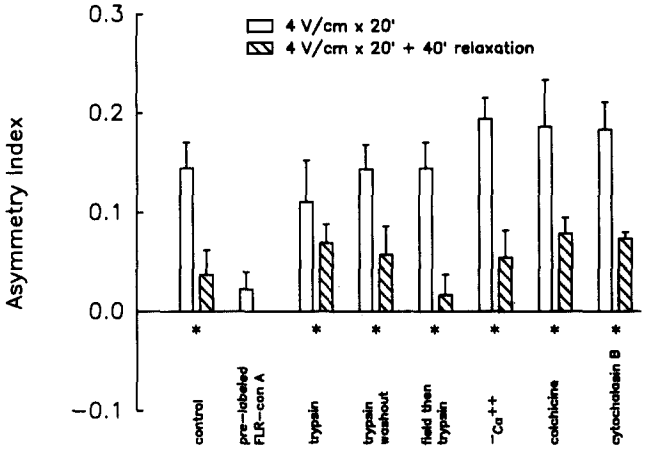

Figure 12. The effects of treatments on the electrophoresis and relaxation of con A binding sites. Cultures were treated as indicated and subjected to a field of 4 V/cm for 20 min with and without an additional 40 min of relaxation. Except where noted the cells were then double labeled and analyzed as described. Control, no additional treatment. Pre-labeled FLR-con A, incubated with 25 μg/ml FLR-con A for 10 min at 22°C and then electrophoresed (no further labeling). Other treatments, as in Fig. 11 legend. Data represent the means ± SEM of 2–5 experiments, each consisting of 5–9 cells. (*) Indistinguishable from controls (both field and postfield) on the basis of one-factor ANOVA F tests (field, $F_{(5/9)} = 0.97$; postfield $F_{(6/11)} = 0.99$). Within this "control" group, field vs. postfield asymmetry values are significantly different (0.160 ± .013 vs. 0.055 ± .008; $p < 0.001$, *T* test). The mean asymmetry of the control group after the field is significantly different from the mean for pre-labeled FLR-con A ($p < 0.001$, *T* test).

sum of the unnormalized sector intensities weighted by the respective sector areas) was compared in cells subjected to different steady-state field protocols. There was no significant difference between intensity values of cells subjected to electrophoresis at 0, 1, 2, 4, or 8 V/cm, nor was there a significant trend in these values ($p > 0.1$, *T* test; $r^2 = .038$; range = 95–105% of average, $n = 6$–9 cells per condition). Thus, it is unlikely that there is significant deviation from linearity in ligand binding.

Close examination of the data in Fig. 7 *a–c* reveals a small, but systematic deviation from the predicted distributions; the data tend to be low and high in regions around 60° and 120°, respectively. This may be due to an imperfectly cartesian arrangement of the camera pixels in visual space, which would cause a systematic bias in the selection of pixels representing the cell perimeter. The distortion is minor with respect to the changes in site density seen in these experiments (e.g., Fig. 7 *a–d*), and can safely be ignored.

Redistribution of FLR-Con A–binding Sites

Estimates of the diffusion constant for the "average" con A site were made in two different ways: (*a*) from the time course of asymmetry development during exposure to fields (Fig. 4), and (*b*) from the time course of postfield relaxation (Fig. 5). The two methods are in good agreement, yielding $D \approx 2.3 \times 10^{-9}$ cm²/s. This value is in the range reported ($5–50 \times 10^{-10}$ cm²/s for con A site diffusion measured via postfield relaxation in *Xenopus* myoball cultures (Poo et al., 1978, 1979). The range of previously reported values is considerable, and probably due in part to differences in the developmental state of the cultured cells. In the related issue of AChR diffusion, for example, Orida and Poo (1980) have shown a decrease in mobility with age in culture.

The steady-state model describing the electrophoretic distribution of ideal (noninteracting) sites put forth by Jaffe (1977) describes the experimental distribution of con A sites quite well over a fourfold range of field strengths (Fig. 7). In fact the behavior of con A–binding sites at or below 4 V/cm appears ideal both in terms of steady-state distribution and relaxation to near symmetry (Fig. 5). Taking $D = 2.3 \times 10^{-9}$ cm²/s, and $m/D = 64$ V^{-1} (Fig. 7), we arrive at an estimate of $m = 1.5 \times 10^{-7}$ cm²/V · s. Values for *m* reported by Poo et al. (1978, 1979) are $\sim 2 \times 10^{-7}$ cm²/V · s, in good agreement with this result. However, estimates for *m* depend critically on assumptions about f_m, the fraction of sites that are free to move. This value cannot be

rigorously estimated by the present techniques, as the predicted distributions over the range of ideal behavior are quite similar (see legend to Fig. 7). It has been argued that f_m can be estimated from the maximum asymmetry seen with increasing field strengths (Poo et al., 1979). However, our data suggest that the behavior of con A sites at higher field strengths is nonideal (see Fig. 8 and below), and accordingly that such an estimate may be misleading. Given the multiplicity of factors required for rigorous estimation of m and D, the estimated values are less noteworthy than the observation that the same parameter values can successfully describe the experimental distributions over a significant range of field strengths.

The lack of correspondence between theory and observation at 8 V/cm is deserving of further comment. Two lines of evidence suggest non-ideal behavior under these conditions. First, and as seen by Poo et al. (1978), relaxation is incomplete after exposure to such a field (Fig. 5). Second is the finding that parameters characterizing steady-state distributions from lesser voltage gradients do not adequately describe the results seen at 8 V/cm under steady-state conditions; the asymmetry at 8 V/cm is less than would be expected (Fig. 8). Using different techniques to assay FLR-con A binding, Poo et al. (1979) concluded that the distributions of FLR-con A sites correspond to theory reasonably well in a range of fields up to 10 V/cm.

The apparent discrepancy documented here could in principle arise from nonlinear ligand binding, or concentration-dependent quenching effects, revealed at the higher binding-site concentrations found in the 8 V/cm condition. Inspection of Fig. 8, however, shows that even within the range of intensities found at 4 V/cm ($\theta \approx 50$–$150°$), the 8 V/cm data do not correspond to the theoretical expectation. Thus, although such effects cannot be ruled out, neither can they account for the differences seen between the two experimental conditions.

There are several possible biophysical explanations for the reduction of experimental asymmetry at higher field strengths. One possibility is that under these conditions the mobility of the con A sites is reduced. The time course at 8 V/cm (Fig. 4) contradicts a simple version of this proposal, but an accumulation-dependent decrease in mobility could lead to an underestimate of the time required to reach steady-state. A second explanation is that electrostatic interactions, not accounted for in the model, play a role when asymmetries become large. There are reasons to believe such effects would be small under most conditions (e.g., a Debye length of ~1 nm in physiological saline[4]), but without knowing the concentrations and mobilities of all charged species involved, the possibility cannot be ruled out. A third argument challenges the assumption, inherent in the model, that the cell is closely approximated by a nonconducting sphere. At 8 V/cm, an iso-potential cell of radius 20 μm will experience 16 mV hyper- and depolarizations at the anode and cathode ends, respectively. These may lead to changes in membrane conductance due to the presence of voltage-sensitive channels, and thereby violate the validity of the approximation. Although predictions about the resulting distribution of sites at steady-state would require precise knowledge of the densities and responses of such channels (which might themselves migrate in a field) the influence would be in the observed direction, that is, it would lead to a decrease in the observed asymmetry. Finally, as noted in footnote 2, the driving force may be electro-osmotic. A consequence of this is that redistribution of surface charge could diminish the driving force experienced by sites at the pole to which they are driven. A related effect is the possible establishment of a pH gradient on the cell surface, leading to a change in the charge carried by con A sites near the poles.

Redistribution of AChRs

In contrast to the case for the heterogeneous population of con A–binding sites, there are no conditions under which the AChR shows ideal behavior vis a vie the proposed model. Evidence for interaction among AChRs subjected to electrophoresis comes from the nonexponential rise in asymmetry with time (data not shown), the distribution after exposure to a field (Fig. 9), and the continued increase in AChR asymmetry after removal from the electric field (see below).

Two points emerge from analysis of the data in Fig. 9, which shows the distribution of AChRs seen after 80 min in an 8 V/cm field. First, the steady-state family of distributions from the model under consideration cannot adequately represent the observed distribution; to achieve even a poor fit the m/D parameter has to become quite large, and f_m is forced to be very small. A second point is that the minimum AChR density (at ~100–130°) is adjacent to the region of AChR accumulation, whereas the steady-state model predicts the minimum should be at the anode-facing pole. The location of this minimum suggests the operation of a diffusion-trap mechanism (Edwards and Frisch, 1976), in which immobilization of AChRs at the cathode-facing pole leads to depletion in neighboring regions via diffusion-mediated migration. The location of this minimum would not be expected from a cell-wide cytoskeletal rearrangement of sites, although a locally confined mechanism of this sort cannot be ruled out.

In any event, it is clear that the distribution seen in Fig. 9 results from more than just the ideal behavior assumed by the model. The contribution made to the distribution of Fig. 9 by this ideal behavior can be roughly estimated by assuming that the effect accounts for 100% of the decrease in AChR density seen at the anode-facing pole. The dashed-line curve in Fig. 9 was fitted by eye with this in mind, and serves to illustrate graphically the minor role of electrophoretic migration per se under these conditions. This is in agreement with results showing similarity between asymmetries from experiments at 8 V/cm for 80 min (Fig. 9: $A = .55 \pm .06$), and at 8 V/cm for 20 min + 60 min relaxation (data not shown): $A = 0.42 \pm .05$). Thus, the mechanism(s) underlying the postfield accumulation, discussed below, can dominate the distribution even in the presence of an electric field.

A field/postfield experimental protocol was devised to isolate the postfield aggregation phenomenon for further study. Analysis of con A site distribution under this paradigm shows the expected decrease in asymmetry during the postfield period; none of the applied treatments significantly altered the decrease (Fig. 12). In contrast, the results shown

4. Note however, that the charges within or very near the membrane will interact significantly at distances greater than the aqueous phase Debye length.

in Fig. 10 and 11 demonstrate an increased accumulation of AChRs during the postfield period, as had been suggested by the data of Orida and Poo (1981).

That this aggregation is due to recruitment of AChRs already expressed on the cell surface is shown by experiments in which pre-existing AChRs were labeled with TMR-α-Bgt, and then analyzed with the field/postfield protocol (Fig. 11). These results rule out the possibility that the effect is solely due to preferential insertion of AChRs at the cathode. Experiments in which cells were preincubated with con A and then treated with electric fields show no evidence of localized expression of new AChRs during the hour-long course of these experiments (Fig. 11).

Previous experiments have shown that trypsin inhibits field-induced AChR aggregation, and disperses preexisting accumulations (Orida and Poo, 1980, 1981). Accordingly, experiments were undertaken to analyze the effects of trypsin on the postfield accumulation of AChRs. Trypsin digestion throughout the experiment, as a pretreatment, or at the start of the postfield period greatly reduced the asymmetry seen after the postfield period (Fig. 11). In the first two paradigms the asymmetries seen immediately after the field were also significantly reduced, in agreement with the analysis (above), suggesting that a field-independent aggregation process dominates during exposure to fields. Although it is difficult to rule out indirect intracellular effects, or effects on AChR electrophoretic mobility, the most likely mechanism for the action of trypsin is a direct disruption of adhesion or cohesion events stabilizing AChR clusters.

The effects of low calcium on AChR accumulation are less dramatic and more difficult to interpret in a mechanistic sense. Cells incubated in Ca^{++}-free Steinberg's solution show a decreased asymmetry in both field and postfield conditions compared with control cultures (Fig. 11). Low calcium can cause differences in charge density at the surface of the membrane (McDaniel and McLaughlin, 1985), and thus could affect the electrophoretic mobility of AChRs. However, the observed asymmetry in low calcium experiments is still greater than the estimated electrophoretic contribution, suggesting that calcium must in part affect the aggregation phenomenon. The partial reversal of the calcium effect, seen in both field and postfield protocols, is consistent with this in light of the argument (above) that aggregation dominates the distribution even in the field (only) protocol. The observed effects could be based on calcium-dependent intracellular events, or calcium-mediated adhesion events (cf. Takeichi, 1977; Grunwald et al., 1980; Brackenbury et al., 1981). In the context of the effects of trypsin the latter interpretation is simplest, though the role of calcium in regulating myriad intracellular events prevents exclusion of this set of possibilities. Leaving aside mechanistic questions, the observation of reduced accumulation is in accord with the observed effects of low calcium on AChR clustering in neural and aneural *Xenopus* muscle cultures (Henderson et al., 1984; Davey and Cohen, 1986), as well as clustering induced by latex beads (Peng, 1984).

The results of experiments with cytoskeleton-disrupting drugs indicate that rearrangement of microtubules and microfilaments is not required for the aggregation effect documented here (Fig. 11). In contrast colchicine, but not cytochalasin B, decreased AChR cluster number and reduced recovery of cluster number following treatment with azide, in a 6-h assay on cultured rat myotubes (Bloch, 1979). Experiments by Connolly (1984) demonstrated that cytochalasins disrupt preexisting AChR clusters in aneural chick muscle cultures over a period of 24 h, and that both cytochalasins and Colcemid prevent an increase in cluster number during the 6 h after addition of brain extract. Others have suggested cytoskeletal anchoring of AChR clusters as evidenced by the protection of clustered AChRs from detergent extraction (Prives et al. 1980, 1982; Stya and Axelrod, 1983).

Methodological differences may account for these apparent discrepancies. In the works of Bloch (1979) and Connolly (1984) it is cluster number that is being assayed, whereas our results speak directly to the question of AChR accumulation. In this context, Bloch (1979) has noted that drugs inhibiting re-clustering of AChRs seem to block the initial formation of foci, and that after foci formation, clustering proceeded in the presence of drugs. Most clusters in aneural cultures are found in regions of close contact between cell and substrate (Bloch, 1980). Thus, it may be that cytoskeletal involvement is required for such contacts, which serve to trigger foci formation (see Connolly, 1984). In contast to these kinds of experiments, the accumulation event reported here is removed from regions of cell attachment. Put in more general terms, it may be that any of several unrelated in vitro manipulations can trigger accumulation. Under these circumstances, interpretation regarding in vivo mechanisms is difficult (see Fraser and Poo, 1982). A second point is the difference in time-scale of the experiments under discussion. It is possible that early events in AChR aggregation, themselves independent of the cytoskeleton, may lead to secondary stabilization via microtubules and/or microfilaments. Thus, experiments may give rise to different interpretations depending on how long after initial cluster formation the study is carried out. Finally, different species were used in these experiments. Though it is tempting to think that underlying mechanisms for phenomenologically similar events would be conserved, this need not be the case.

Taken together, our data are consistent with a simple interpretation of the events required for initial AChR accumulation: the AChR migrates in response to the electric field, and the local increase in AChR concentration at the cathode-facing pole activates a diffusion-trap mechanism. The trapping mechanism is calcium sensitive and trypsin labile, and is insensitive to colchicine and cytochalasin B. If the triggering event is simply the increase in local AChR concentration, the average concentration of AChRs before experimental manipulation is probably near threshold; shown in Fig. 9 (*dashed line*) is a crude estimate of the increase in AChR concentration due to the field alone. An interesting alternative view, indistinguishable from the above given the present data, is that electrophoretic migration of some other species results in the accumulation of components necessary for the trapping mechanism. Work underway in several laboratories is directed toward characterization of factors which may play a role in AChR clustering (for review see Schuetze and Role, 1987); factors such as these may interact with membrane components responsible for the accumulation documented here.

Is the diffusion of AChRs sufficiently rapid to account for the observed rate of aggregation via a diffusion-trap mechanism? The AChR diffusion constant was measured in *Xenopus* cultures by the recovery of sensitivity after local inacti-

vation with α-Bgt, and found to be 2.6×10^{-9} cm²/s (Poo, 1982). Two other parameters critical to estimation of trapping rate must be assumed; these are the trap size[5] and the trapping efficiency (see Chao et al., 1981 and Weaver, 1983). Following Weaver (1983), and with the simple assumptions that the trap is 100% efficient and the trap size is 3 sectors ($\theta = 33.75°$—see Fig. 9), we find the mean trapping time (i.e., the time after which half of the AChRs would be trapped) to be ~4 min. Analysis of the data of Fig. 9 shows that, taking sectors 14–16 to represent the trap, only ~9% of the sites from the rest of the cell surface have been confined to the trap region after 80 min. Thus, diffusion of AChRs is easily fast enough to account for the observed aggregation. This conclusion is in accordance with results from Kuromi et al. (1985), in which the accumulation of AChRs at neuromuscular contacts was characterized using *Xenopus* cultures. It should be noted that use of fluorescence photobleaching recovery techniques to measure the AChR diffusion constant in *Xenopus* cultures gives a result ~10-fold lower than that used in this calculation (see Kuromi et al., 1985, for discussion of intrinsic differences between these methods). However, even using this much lower estimate, the rate of diffusion is greater than that needed to account for the observed accumulation. The fact that the experimental aggregation is considerably slower than that predicted in this calculation implies that, if the diffusion-trap mechanism is operative, the trap is less than 100% efficient, or the trap size is less than 33.75°, or both.

A further test of the diffusion-trap proposal would be to examine whether the aggregation can occur in the absence of metabolic energy sources. Attempts were made to test this by administration of drugs interfering with ATP synthesis. Unfortunately, the time required for consistent, complete loss of acetylcholine-induced twitch response was ~1.5 h, and the cells began to lyse shortly thereafter. Thus, conclusive testing of this prediction could not be performed.

General Conclusions

Our experimental findings suggest that the data analysis techniques presented here constitute a valid and powerful tool for the examination of factors contributing to the distribution and migration of membrane components. We find support for a model based on electrophoresis and diffusion (Jaffe, 1977) in the behavior of con A–binding sites over a fourfold range of electric field strengths. At a higher field strength the description of con A site behavior breaks down, presumably due to the failure of assumptions on which the model is based.

The AChR is not well described by this model under any of the conditions examined, apparently because of interactions between the AChRs (and possibly other surface components). These interactions are probably mediated by a local increase in the concentration of AChRs or other components, which triggers an aggregation event independent of microtubule or microfilament rearrangements. It is possible that multiple in vitro manipulations can trigger the accumulation of AChRs. Our data are consistent with a description of the aggregation phenomenon as one driven by a passive, diffusion-trap mechanism. The aggregation behavior reported here is suggestive in light of the in vivo accumulation of AChRs at the developing neuromuscular junction, and may play a significant role in the initial events responsible for AChR clustering.

We thank Drs. Darwin Berg and Stanley Halvorsen for advice and aid in the fluorescent labeling of α-Bgt.

This work was supported by a grant from the Monsanto Corporation, a National Institutes of Health (NIH) Training grant (HD07029) (J. Stollberg), and by a McKnight Scholar Award (S. Fraser).

Received for publication 30 November 1987, and in revised form 21 January 1988.

References

Anderson, M. J., M. W. Cohen, and E. Zorychta. 1977. Effects of innervation on the distribution of acetylcholine receptors on cultured muscle cells. *J. Physiol (Lond.)* 268:731–756.

Bloch, R. J. 1979. Dispersal and reformation of acetylcholine receptor clusters on cultured rat myotubes treated with inhibitors of energy metabolism. *J. Cell Biol.* 82:626–643.

Bloch, R. J., and B. Geiger. 1980. The localization of acetylcholine receptor clusters in areas of cell-substrate contact in cultures of rat myotubes. *Cell.* 21:25–35.

Boulter, J., and J. Patrick. 1979. Concanavalin A inhibition of α-Bungarotoxin binding to a nonfusing muscle cell line. *J. Biol. Chem.* 254:5652–5657.

Brackenbury, R., U. Rutishauser, and G. M. Edelman. 1981. Distinct calcium-independent and calcium-dependent adhesion systems of chicken embryo cells. *Proc. Natl. Acad. Sci. USA.* 8:387–391.

Chao, N-m., S. H. Young, and M-m. Poo. 1981. Localization of cell membrane components by surface diffusion into a "trap." *Biophys. J.* 36:139–153.

Connolly, J. A. 1984. Role of the cytoskeleton in the formation, stabilization, and removal of acetylcholine receptor clusters in cultured muscle cells. *J. Cell Biol.* 99:148–154.

Davey, D. F., and M. W. Cohen. 1986. Localization of acetylcholine receptors and cholinesterase on nerve-contacted and noncontacted muscle cells grown in the presence of agents that block action potentials. *J. Neurosci.* 6:673–680.

Edidin, M. 1975. Rotational and translational diffusion in membranes. *Annu. Rev. Biophys. Bioeng.* 3:179–201.

Edwards, C., and H. L. Frisch. 1976. A model for the localization of acetylcholine receptors at the muscle endplate. *J. Neurobiol.* 7:377–381.

Fraser, S. E., and M.-m. Poo. 1982. Development, maintenance, and modulation of patterned membrane topography: models based on the acetylcholine receptor. *Curr. Top. Dev. Biol.* 17:77–100.

Frye, L. D., and M. Edidin. 1970. The rapid intermixing of cell surface antigens after formation of mouse-human heterokaryons. *J. Cell. Sci.* 7:319–335.

Grunwald, G. B., R. L. Geller, and J. Lilien. 1980. Enzymatic dissection of embryonic cell adhesive mechanisms. *J. Cell Biol.* 85:766–776.

Henderson, L. P., M. A. Smith, and N. C. Spitzer. 1984. The absence of calcium blocks impulse-evoked release of acetylcholine but not *de novo* formation of functional neuromuscular synaptic contacts in culture. *J. Neurosci.* 4:3140–3150.

Huang, N. W. 1973. Mobility and diffusion in the lane of cell membrane. *J. Theor. Biol.* 40:11–16.

Jaffe, L. F. 1977. Electrophoresis along cell membranes. *Nature (Lond.).* 265: 600–602.

Kuromi, H., and Y. Kidokoro. 1984. Nerve disperses preexisting acetylcholine receptor clusters prior to induction of receptor accumulation in *Xenopus* muscle cultures. *Dev. Biol.* 103:53–61.

Kuromi, H., B. Brass, and Y. Kidokoro. 1985. Formation of acetylcholine receptor clusters at neuromuscular junction in *Xenopus* cultures. *Dev. Biol.* 109:165–176.

Lin-Liu, S., W. R. Adey, and M.-m. Poo. 1984. Migration of cell surface concanavalin A receptors in pulsed electric fields. *Biophys. J.* 45:1211–1218.

Marchesi, V. T. 1985. Stabilizing infrastructure of cell membranes. *Annu. Rev. Cell Biol.* 1:531–561.

McDaniel, R., and S. McLaughlin. 1985. The interaction of calcium with gangliosides in bilayer membranes. *Biochim. Biophys. Acta.* 819:153–160.

McLaughlin, S., and M.-m. Poo 1981. The role of electro-osmosis in the electric-field-induced movement of charged macromolecules on the surfaces of cells. *Biophys. J.* 34:85–93.

Nieuwkoop, P. D., and J. Faber. 1962. Normal table of *Xenopus laevis.* North Holland Publishing Co., Amsterdam.

Orida, N., and M.-m. Poo. 1978. Electrophoretic movement and localization of acetylcholine receptors in the embryonic muscle cell membrane. *Nature (Lond.).* 275:31–35.

5. The region of high AChR density in Fig. 9 (sectors 13–16) might represent a single trap, or many small micro-aggregates; hence the trap size cannot be ascertained from the distribution.

Orida, N. and M.-m. Poo. 1980. On the developmental regulation of acetylcholine receptor mobility in the *Xenopus* embryonic muscle membrane. *Exp. Cell Res.* 130:281–290.

Orida, N., and M.-m. Poo. 1981. Maintenance and dissolution of acetylcholine receptor clusters in the embryonic muscle cell membrane. *Dev. Brn. Res.* 1:293–298.

O'Rourke, N. A., and S. E. Fraser. 1986. Dynamic aspects of retinotectal map formation revealed by a vital-dye fiber-tracing technique. *Dev. Biol.* 114: 265–276.

Peng, H. B. 1984. Participation of calcium and calmodulin in the formation of acetylcholine receptor clusters. *J. Cell Biol.* 98:550–557.

Peng, B. H. M., and L. F. Jaffe. 1976. Polarization of fucoid eggs by steady electrical fields. *Dev. Biol.* 53:277–289.

Poo, M.-m. 1981. In situ electrophoresis of membrane components. *Annu. Rev. Biophys. Bioeng.* 10:245–276.

Poo, M.-m. 1982. Rapid lateral diffusion of functional ACh receptors in embryonic muscle cell membrane. *Nature (Lond.).* 295:332–335.

Poo, M.-m., and R. A. Cone. 1974. Lateral diffusion of rhodopsin in the photoreceptor membrane. *Nature (Lond.).* 247:438–441.

Poo, M.-m., and K. R. Robinson. 1977. Electrophoresis of concanavalin A receptors along embryonic muscle cell membrane. *Nature.* 265:602–605.

Poo, M.-m., W-j. H. Poo, and J. W. Lam. 1978. Lateral electrophoresis and diffusion of concanavalin A receptors in the membrane of embryonic muscle cell. *J. Cell. Biol.* 76:483–501.

Poo, M.-m., J. W. Lam, N. Orida, and A. W. Chao. 1979. Electrophoresis and diffusion in the plane of the cell membrane. *Biophys. J.* 26:1–22.

Press, W. H., B. P. Flannery, S. A. Teukolsky, and W. T. Vetterling. 198(Numerical Recipes. Cambridge University Press, New York. 1–818.

Prives, J. C., C. S. Penman, and K. Olden. 1980. Neuronal regulation of mu cle acetylcholine receptors: role of muscle cytoskeleton and receptor carb hydrate. *In* Tissue Culture in Neurobiology. E. Giacobini, A. Vernadaki and A. Shahar, editors. Raven Press, New York. 35–52.

Prives, J., A. B. Fulton, S. Penman, M. P. Daniels, and C. N. Christian. 198 Interaction of the cytoskeletal framework with acetylcholine receptor on tl surface of embryonic muscle cells in culture. *J. Cell Biol.* 92:231–236.

Ravdin, P., and D. Axelrod. 1977. Fluorescent tetramethyl rhodamine deriv tives of alpha-Bungarotoxin: Preparation, separation, and characterizatio *Analyt. Biochem.* 80:585–592.

Role, L. W., V. R. Matossian, R. J. O'Brien, and G. D. Fischbach. 1985. C the mechanism of acetylcholine receptor accumulation at newly formed sy apses on chick myotubes. *J. Neurosci.* 5:2197–2204.

Schuetze, S. M., and L. W. Role. 1987. Developmental regulation of nicotin acetylcholine receptors. *Annu. Rev. Neurosci.* 10:403–457.

Singer, S. J., and G. L. Nicholson. 1972. The fluid mosaic model of the stru ture of cell membranes. *Science (Wash. DC).* 175:720–731.

Takeichi, M. 1977. Functional correlation between cell adhesive properties ar some cell surface proteins. *J. Cell Biol.* 75:464–474.

Weaver, D. L. 1983. Diffusion-mediated localization on membrane surface *Biophys. J.* 41:81–86.

Ziskind-Conhaim, L., I. Geffen, and Z. W. Hall. 1984. Redistribution of ac tylcholine receptors on developing rat myotubes. *J. Neurosci.* 4:2346–234